ELSEVIER

Catalysis Today 67 (2001) 205–216

CATALYSIS TODAY

www.elsevier.com/locate/cattod

Investigation of mass transfer through inorganic membranes with several layers

S. Thomas [a,*], R. Schäfer [b], J. Caro [b], A. Seidel-Morgenstern [a,c]

[a] *Otto-von-Guericke-Universität Magdeburg, Institut für Verfahrenstechnik, D-39106 Magdeburg, Germany*

[b] *Institut für Angewandte Chemie Berlin-Adlershof e.V., Richard-Willstätter-Str. 12, D-12489 Berlin, Germany*

[c] *Max-Planck-Institut für Dynamik komplexer technischer Systeme, D-39120 Magdeburg, Germany*

Abstract

Suitable porous membranes for application in membrane reactors usually consist of several layers. The selective separation layer is in general deposited on one or several supporting layers having larger pores. For the sake of simplicity the mass transfer through such composites is frequently modelled using integral parameters. However, this simplified description has serious limitations, e.g. it is not capable to quantify the often observed effects of direction dependencies of flow and selectivity. In this paper the mass transfer is studied simultaneously to the production process of asymmetric membranes. Membranes made of different α- and γ-alumina layers were prepared. In a final preparation step a further silica sol–gel layer was deposited. To characterise the membranes SEM, EDX, ^{29}Si-NMR and permeation measurements were applied. After each deposition of a new layer, permeation was studied and analysed in order to determine characteristic parameters of this layer assuming the parameters of the previous layers to be known. The dusty gas model could be applied successfully for the quantification of the mass transfer through the multi-layer alumina membranes. Using the determined model parameters for all alumina layers, internal pressure profiles were simulated for the two possible flow directions. The differences of fluxes for the same total pressure gradients were quantified. The mass transfer through the finally deposited sol–gel layer was found to be more complex. A qualitative description based on the concept of configurational diffusion was performed. All results obtained emphasise the necessity of taking membrane asymmetries properly into account during the design and analysis of membrane reactors.

Keywords: Layer; Mass transfer; Inorganic membranes

1. Introduction

Due to their outstanding thermal and chemical stability inorganic membranes are promising candidates to be applied in membrane reactors [1]. Potential fields are to use membranes in order to remove selectively products of equilibrium controlled reactions (e.g. for dehydrogenation [2–5]) or to dose reactants in an optimised manner in order to improve the selectivities of consecutive reactions (e.g. for the oxidative coupling of methane [6–8]). Despite numerous successful demonstrations of membrane reactors in the laboratory scale, up to now no large scale membrane reactor has been realised. Main hurdles are (i) insufficient properties of the available membranes (limited fluxes and

* Corresponding author. Tel.: +49-391-67-18643; fax: +49-391-67-12028.
E-mail addresses: sascha.thomas@vst.uni-magdeburg.de (S. Thomas), schaefer@aca-berlin.de (R. Schäfer), caro@aca-berlin.de (J. Caro), anseidel@vst.uni-magdeburg.de (A. Seidel-Morgenstern).

0920-5861/01/$ – see front matter
PII: S0920-5861(01)00288-7

Nomenclature

B_0^e	permeability constant (m^2)
d_P	mean pore diameter (m)
D_{ij}	binary diffusion coefficient (m^2/s)
D_i^c	diffusion coefficient of configurational diffusion (m^2/s)
$D_{K,i}^e$	Knudsen diffusion coefficient (m^2/s)
E_i^C	activation energy of configurational diffusion (J/mol K)
J	molar flux density (mol/s m^2)
k_0^e	Knudsen coefficient (m)
L	membrane length (m)
M	molar mass (kg/mol)
$\dot{n}$	molar flux (mol/s)
p	pressure (Pa)
r	radius (m)
$\Re$	universal gas constant (J/mol K)
T	temperature (K)
x	mole-fraction

Greek symbols

ε	porosity
η	viscosity (Pa s)
ρ_g	probability factor
τ	tortuosity

selectivities, poor mechanical stabilities), (ii) problems in describing properly the mass transfer through the membranes and the interplay with the chemical reactions and (iii) limited scale-up experiences. Extensive overviews concerning the present state of the development of membrane reactors were recently published [9–12].

In this paper exclusively aspects of quantifying the mass transfer through multi-layer porous membranes are addressed. Such membranes are usually prepared as composites consisting of one or several support layers providing the mechanical stability and a separation layer providing the required selectivity. Often the main transport resistance is in the separation layer which for this reason should be very thin. Obviously, this tendency is restricted by the increasing occurrence of defects. An important consequence of the application of thin separation layers is the fact that the relative resistance of the thicker support layer becomes more significant again. For this reason composite membranes consisting of layers of different thickness and porosities often exhibit direction dependent fluxes due to non-symmetric internal pressure profiles [13]. Unfortunately, in general such internal profiles cannot be measured using the final membrane materials. For this reason in [14] a special diffusion cell was applied in which flat membranes were arranged in a sandwich like manner. This cell allowed to measure the pressure drops between the individual layers for two flux directions. An alternative approach was chosen in this work. The transport properties of tubular composite membranes were studied simultaneously to the manufacturing process. Different alumina sols were used producing an non-symmetric membrane on an alumina support with high porosity. Finally, the obtained ultrafiltration membrane was dip-coated with a silica sol developing a microporous membrane for gas separation. Besides characterising the transport through the individual layers the influence of the flow direction on the magnitude of fluxes was quantified.

2. Mass transfer in porous media

There are several excellent reviews available analysing the mass transfer in porous media [15–17]. Although modern concepts orient on the application of more complex network models [18] it is widely accepted that the mass transfer in a large range of pore sizes can be quantified in a simple manner satisfactory using the dusty gas model (DGM [15]). This model takes into account molecular and Knudsen diffusion as well as the contributions of viscous flux. However, in the region of micropores other effects begin to dominate and different models have been suggested. One of the most advanced concepts is based on the assumption of activated configuration diffusion in these small pores [19,20]. Below the key equations of the DGM and the model of configuration diffusion are summarised.

2.1. Dusty gas model (DGM)

The DGM is frequently used to model the multicomponent mass transfer through ceramic membranes. The main model equation capable to predict molar flux

densities J_i for all components is [15]

$$-\frac{p}{\Re T}\nabla x_i - \frac{x_i}{\Re T}\left(1+\frac{B_0^{\mathrm{e}}}{D_{\mathrm{K},i}^{\mathrm{e}}\eta}p\right)\nabla p = \sum_{j=1,j\neq i}^{n}\frac{x_j J_i - x_i J_j}{D_{ij}^{\mathrm{e}}} + \frac{J_i}{D_{\mathrm{K},i}^{\mathrm{e}}}, \quad i=1,n \tag{1}$$

with

$$D_{\mathrm{K},i}^{\mathrm{e}} = \frac{4}{3}k_0^{\mathrm{e}}\sqrt{\frac{8\Re T}{\pi M_i}} \tag{1a}$$

$$D_{ij}^{\mathrm{e}} = \frac{\varepsilon}{\tau}D_{ij} \tag{1b}$$

Three gas phase transport mechanisms are considered by this model:

- Molecular diffusion;
- Knudsen diffusion;
- Viscous flux.

The left side of Eq. (1) quantifies the driving forces formed by partial pressure and overall pressure differences across the membrane. The first term on the right side takes into account interactions between the molecules in the gas phase. The second term considers the resistance between the molecules in the gas phase and the solid assumed to consist of regularly distributed dust molecules fixed in space.

The binary diffusion coefficient D_{ij} can be estimated using the Chapman–Enskog equation [21]. The three membrane parameters of the DGM, i.e. the Knudsen coefficient k_0^{e}, the permeability constant B_0^{e} and the ratio of porosity to tortuosity ε/τ, have to be determined experimentally.

If a single gas permeates through a membrane the DGM reduces to:

$$J_i = -\frac{1}{\Re T}\left(\frac{4}{3}k_0^{\mathrm{e}}\sqrt{\frac{8\Re T}{\pi M_i}} + \frac{B_0^{\mathrm{e}}}{\eta_i}p\right)\nabla p \tag{2}$$

For a cylindrical membrane after integration the following linear dependence of the ratio of the molar flow rates over the pressure difference, $n_i/\Delta p$, versus the mean pressure $\bar{p}$ holds:

$$\frac{\dot{n}_i}{\Delta p} = -\frac{2\pi L}{\Re T\ln(r_{\mathrm{outer}}/r_{\mathrm{inner}})}\left(\frac{4}{3}k_0^{\mathrm{e}}\sqrt{\frac{8\Re T}{\pi M_i}} + \frac{B_0^{\mathrm{e}}}{\eta_i}\bar{p}\right) \tag{3}$$

The slope of this linear dependence is proportional to the permeability constant, B_0^{e}, and the intercept contains the Knudsen coefficient, k_0^{e}. Knowing k_0^{e} and B_0^{e} and assuming non-interconnected, circular capillaries one can estimate a mean pore diameter [15]

$$d_{\mathrm{P}} = \frac{8B_0^{\mathrm{e}}}{k_0^{\mathrm{e}}} \tag{4}$$

and a mean ratio of porosity to tortuosity

$$\frac{\varepsilon}{\tau} = \frac{(k_0^{\mathrm{e}})^2}{2B_0^{\mathrm{e}}} \tag{5}$$

2.2. Configurational diffusion

If the pore diameters approach the range of the sizes of the molecules mass transfer characteristics change and the configurational diffusion regime is reached where molecules never escape completely from the potential field of the solid [19]. The corresponding flux density can be described in a simplified manner by [20]

$$J_i = -\frac{1}{\Re T}\frac{\varepsilon}{\tau}D_i^{\mathrm{c}}\nabla p_i \tag{6}$$

with

$$D_i^{\mathrm{c}} = \rho_{\mathrm{g}} d_{\mathrm{P}}\sqrt{\frac{8\Re T}{\pi M_i}}\,\mathrm{e}^{-(E_i^{\mathrm{c}}/\Re T)} \tag{6a}$$

There are no well-accepted formulas to predict the diffusivities D_i^{c}. The temperature dependence of these parameters differs completely from the temperature dependence of the Knudsen diffusivities (Eq. (1a)). The parameter ρ_{g} stands for the probability that a gas molecule is capable to surpass the energy barrier E_i^{c}.

In the region of very small pores also the effect of surface diffusion might be significant [22]. Recently in [23] the aspects of broader pore size distributions, mobile adsorbed phases and overlapping transport mechanisms have been analysed in more detail.

2.3. Description of gas permeation through asymmetric porous membranes with the DGM

When a gas permeates through an asymmetric structure consisting out of several porous membranes the

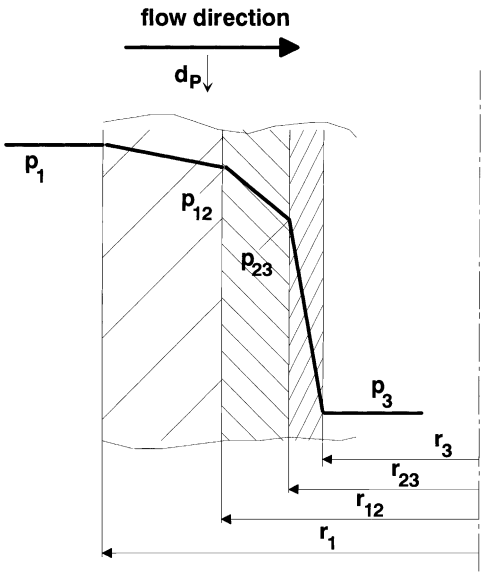

Fig. 1. Pressure profile across an asymmetric membrane (support and two layers), compare Eqs. (7)–(9).

resulting pressure profiles depend on the properties of all layers. Fig. 1 schematically illustrates the situation for a support and two additional layers. Assuming the DGM to be applicable based on Eq. (3) the steady state permeation of a single gas can be described using the following three equations:

$$\frac{\dot{n}_i}{(p_1 - p_{12})} = -\frac{2\pi L}{\Re T \ln(r_1/r_{12})} \times \left(\frac{4}{3} k_0^{\text{e,support}} \sqrt{\frac{8\Re T}{\pi M_i}} + \frac{B_0^{\text{e,support}}}{\eta_i} \frac{p_1 + p_{12}}{2} \right) \tag{7}$$

$$\frac{\dot{n}_i}{(p_{12} - p_{23})} = -\frac{2\pi L}{\Re T \ln(r_{12}/r_{23})} \times \left(\frac{4}{3} k_0^{\text{e,layer 1}} \sqrt{\frac{8\Re T}{\pi M_i}} + \frac{B_0^{\text{e, layer 1}}}{\eta_i} \frac{p_{12} + p_{23}}{2} \right) \tag{8}$$

$$\frac{\dot{n}_i}{(p_{23} - p_3)} = -\frac{2\pi L}{\Re T \ln(r_{23}/r_3)} \times \left(\frac{4}{3} k_0^{\text{e,layer 2}} \sqrt{\frac{8\Re T}{\pi M_i}} + \frac{B_0^{\text{e,layer 2}}}{\eta_i} \frac{p_{23} + p_3}{2} \right) \tag{9}$$

If the geometrical (r_1, r_{12}, r_{23}, r_3) and membrane parameters ($k_0^{e,k}$ and $B_0^{e,k}$) and the pressures p_1 and p_3 are known, it is possible to determine the molar flow rate, $\dot{n}_i$, the intersectional pressures, p_{12} and p_{23}, and thus the whole pressure profile across the membrane.

3. Experimental

3.1. Membrane preparation and characterisation

Ceramic filter membranes were kindly supplied by Hermsdorfer Institut für Technische Keramik (hitk, Hermsdorf, Germany). They had a tubular geometry (length 300 mm, inner/outer diameter approximately 7/10 mm). Starting point was a mechanically stable tubular α-Al_2O_3 support of 1.5 mm wall thickness. The corresponding average pore radii were about 3 mm. On this support three more α-Al_2O_3 layers and one γ-Al_2O_3 layer have been deposited by the supplier (hitk) possessing different thickness and pore radii. Table 1 summarises the multi-layer structure of the membranes investigated. Before a new layer was deposited the membranes were characterised in our lab using permeation experiments as described below.

Ceramic membranes consisting out of the support and four layers are commercially available as micro- and ultrafiltration membranes. However, to separate gases and liquids usually membranes possessing smaller pores in the molecular dimensions are required. Such nanoporous layers can be built up by the sol–gel technique [24,25], by CVD/CVI methods [26], by crystallisation of zeolite layers [27,28] or by a chemical modification of the pore walls [29–32]. Here in our lab the sol–gel method was applied to deposit another nanoporous layer on the available alumina membranes. By acid catalysed hydrolysis of tetraethoxysilane (TEOS) in alcoholic solution SiO_2 polymer sols have been prepared. The SiO_2 gel layers

Table 1
Asymmetric structure of the membranes under study

Layer	Function	Composition	Pore radii[a]	Thickness
Coarse layer	Support	α-Al_2O_3	3 μm	1.5 mm
1st layer		α-Al_2O_3	1 μm	25 μm
2nd layer	Microfiltration	α-Al_2O_3	200 nm	25 μm
3rd layer	Micro/ultrafiltr	α-Al_2O_3	60 nm	25 μm
4th layer	Ultrafiltration	γ-Al_2O_3	6 nm	2–3 μm
5th layer	Nanofiltration/gas-separation	SiO_2		100 nm

[a] Pore radii at 50% of the pore volume (d_{50} data).

have been deposited by a dip coating technique. After drying at room temperature for 2 h, the membranes were calcined at 600°C. Table 2 shows characteristic parameters of the sol–gel technique applied.

In order to characterise the different membranes several standard methods have been applied. Scanning electron microscopy for characterising the support was performed using an Amray 1000 B (Kyky) device at 10 kV with Au coating. To characterise the sols ^{29}Si-NMR spectra were recorded on an Unity Plus 500 (Varian). Scanning electron microscopy with a cold field emission electrode (FE-SEM) was made by a Hitachi S 4100 device at 3 kV without Au coating. Simultaneously, the element composition could be recorded by energy dispersive X-ray spectroscopy (EDX line scan).

3.2. Permeation measurements

For the determination of the membrane parameters a classical steady state permeation experiment was used. The set up is illustrated in Fig. 2. A single gas

Table 2
Characteristic parameters of the sol–gel process applied for the deposition of the SiO_2 layer (layer 5 in Table 1)

Precursor	TEOS (tetraethylorthosilicate)
Temperature of hydrolysis	Room temperature
Ratio water:alkylate	4:1
Catalyst for hydrolysis	HNO_3
Time of ageing	50 h
Viscosity of the SiO_2 sol	1.2–1.5 mPa s
SiO_2 content of the sol	2–4 wt.%
Drying conditions of the coated membrane	2 h at room temperature
Calcination conditions	600°C (6 h), with a heating rate of 0.5°C/min

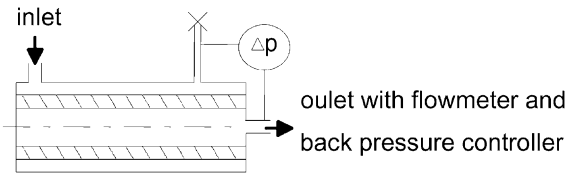

Fig. 2. Set up for the permeation measurements.

permeates through the membrane to be examined and the pressure difference caused by the permeation is measured. A back pressure controller is located at the outlet of the permeation cell. This allows to set different pressure in the cell and thus inside the membrane. The steady state permeation experiment was performed at temperatures between 20 and 500°C and in the pressure range between 1 and 3 bar. As single gases argon, helium, nitrogen and hydrogen were applied.

The described permeation experiment was performed at first to determine the transport properties of the support. Then the coating procedure started. After the deposition of a new layer the permeation properties were investigated again. With the previously determined parameters it was possible to calculate for each experiment the interface pressure between the already characterised membrane and the new layer and thus the parameters of this layer. This procedure was repeated systematically for each subsequent layer of the alumina membranes depicted in Table 1.

4. Results and discussion

4.1. Membrane characterisation

Fig. 3 shows a cross-section of the asymmetric tubular membrane with the support, three α-Al_2O_3 layers

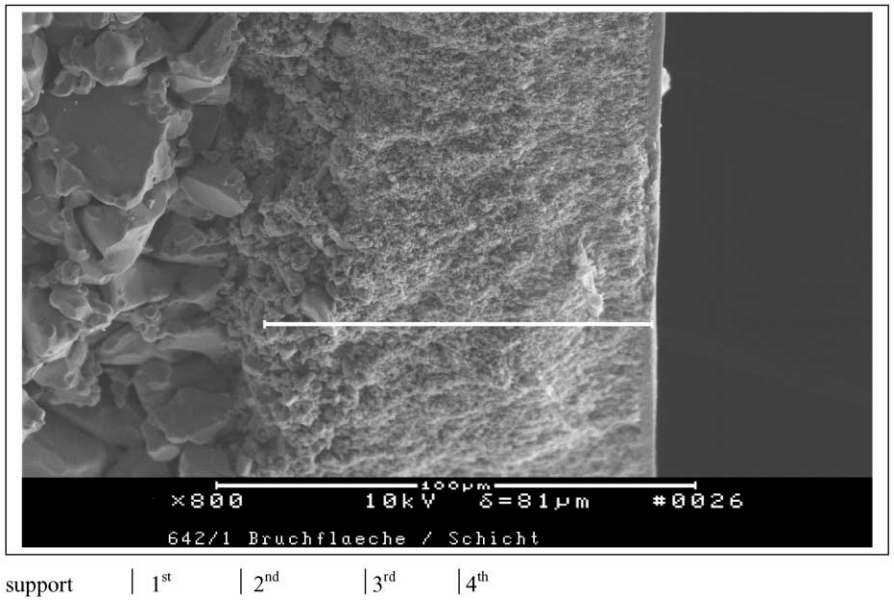

Fig. 3. SEM of the asymmetric alumina membrane.

and the γ-Al_2O_3 toplayer with a thickness of about 2 μm.

The fluxes and selectivities of metal oxide membranes are strongly effected by the parameters of the sol–gel process (Table 2). In particular the degree of branching of the polymeric metal oxides turned out to be very important for the pore sizes. It is known that low branched inorganic polymers lead to gels which can result in membranes with smaller pore size [24,33]. We used ^{29}Si-NMR for characterising the degree of branching of the polymeric SiO_2. Fig. 4 shows the ^{29}Si-NMR spectra of a highly concentrated (12 wt.% SiO_2) SiO_2-sol (50–60 h aged) which was used for membrane preparation after diluting. There are only few Q^4-Si-species ($\delta \sim -110$ ppm) representative of highly branched silica. Most Si-species are Q^3-Si ($\delta \sim -101$ ppm).

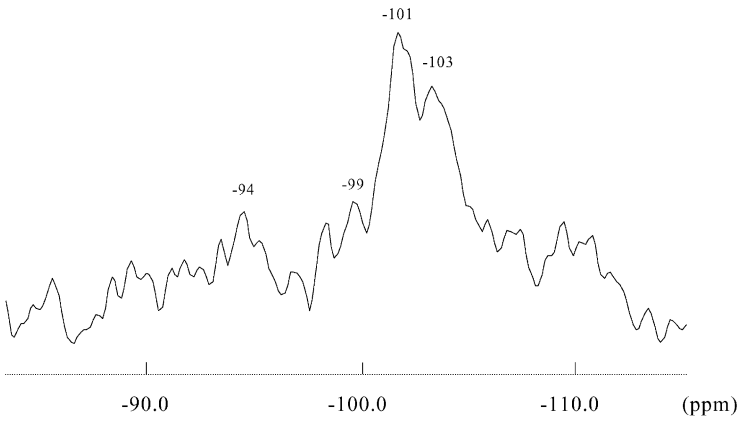

Fig. 4. ^{29}Si-NMR of SiO_2-polymer-sol.

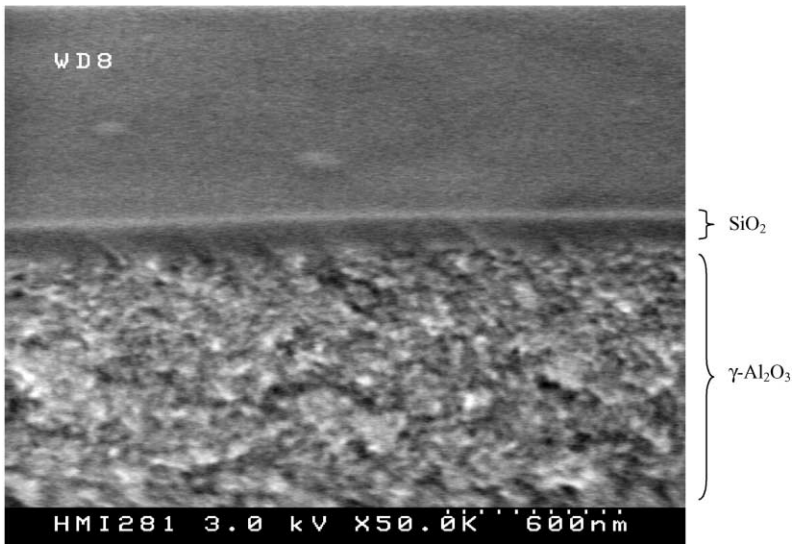

Fig. 5. Electron microscopy. Cross-section of a supported SiO_2-membrane at 50 000-fold magnification.

In Fig. 5 it can be recognised that the alumina layer is completely covered by the silica membrane. The silica membrane has a thickness of about 100 nm after firing treatment at 600°C.

The recorded EDX spectra (Fig. 6) reveal that there is an Si enrichment over 100 nm on the surface of the γ-Al_2O_3 layer which is due to the SiO_2 gel layer. However, there is further detected a remarkable concentration of Si inside the γ-Al_2O_3 layer as well. Obviously, the SiO_2 polymer sol species penetrated into the γ-Al_2O_3 layer during the dip-coating.

4.2. Permeation measurements

The two DGM parameters B_0^e and k_0^e were determined from an analysis of the permeation data for all layers of the asymmetric alumina membrane. The analysis was based on the linearised Eq. (3). The parameters obtained from measurements with different single gases did not differ significantly and were averaged. For each layer the effective pressure differences had to be considered as exemplified by Eqs. (7)–(9) taking the real number of layers into account. The

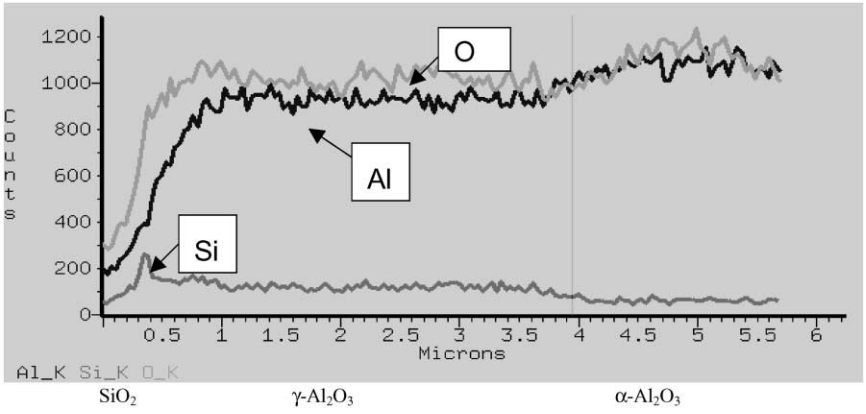

Fig. 6. EDX-spectra from the cross-section of a supported SiO_2-membrane.

Table 3
Determined DGM-parameters of the support and the different layers (averaged for all gases)

	k_0^e (m)	B_0^e (m^2)	ε/τ	Mean pore diameter (μm)
Support	9.34×10^{-8}	3.58×10^{-14}	0.125	3.070
1st layer	4.11×10^{-8}	9.47×10^{-15}	0.164	1.840
2nd layer	9.40×10^{-9}	2.24×10^{-16}	0.188	0.191
3rd layer	5.97×10^{-9}	5.69×10^{-17}	0.398	0.076
4th layer	1.11×10^{-9}	2.18×10^{-18}	0.742	0.016

parameters obtained for the support and the four different layers are summarised in Table 3. Obviously the permeability constant B_0^e and the Knudsen coefficient k_0^e decrease with decreasing pore diameter. From these values the ratio of porosity to tortuosity as well as the mean pore diameter were calculated using Eqs. (4) and (5). Compared to the data of the manufacturer (Table 1) there is a relative good agreement. The larger deviations for the first layer and the γ-alumina layer might be attributable to defects in these layers.

To verify the determined parameters additional steady permeation experiment were analysed. Measured and predicted fluxes through the homogeneous support membrane and a membrane consisting of the support and three layers are shown in Figs. 7–10. The good agreement is not surprising for the support (Figs. 7 and 8) since the data have been used for fitting the parameters. However, also for the membrane with three additional layers (Figs. 9 and 10) the parameter set proves to be capable to describe the situation in the whole temperature and pressure range and for all gases. In agreement with the DGM predictions the fluxes of all gases through both membranes decrease with increasing temperatures and with decreasing pressures.

It can be further noted that the pressure effect is more pronounced for the support due to the larger relative contribution of viscous flux to the overall mass transfer. For the support also the temperature effect is stronger due to the influence of the gas viscosity (increases with temperature). A good agreement between the calculated and measured data can be observed.

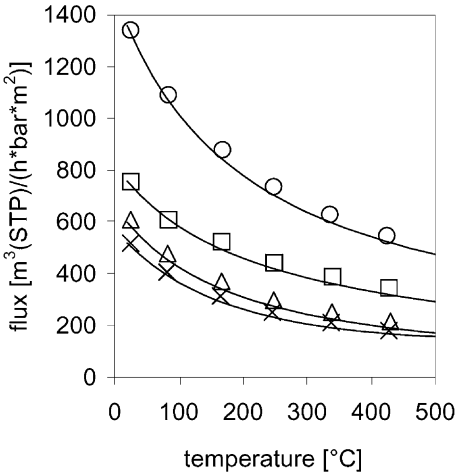

Fig. 7. Flux vs. temperature for the support membrane at 1 bar for hydrogen (○), helium (□), nitrogen (△), argon (×) (lines denote simulation with the determined parameters and symbols denote experimental data).

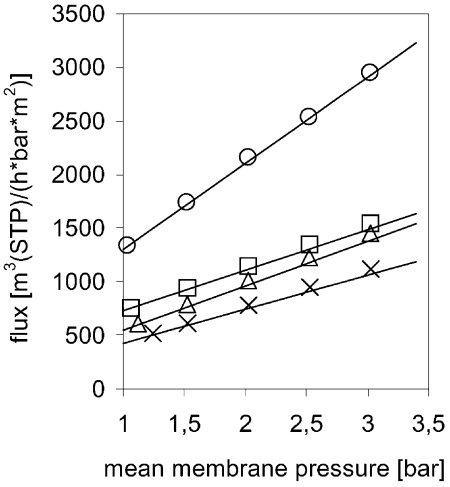

Fig. 8. Flux vs. pressure for the support membrane at 25°C for hydrogen (○), helium (□), nitrogen (△), argon (×) (lines denote simulation with the determined parameters and symbols denote experimental data).

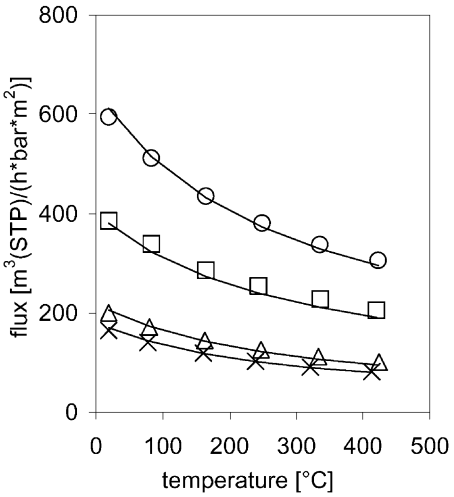

Fig. 9. Flux vs. temperature for the membrane consisting of the support and three layers at 1 bar for hydrogen (○), helium (□), nitrogen (△), argon (×) (lines denote simulation with the determined parameters and symbols denote experimental data).

Due to the performed characterisation of the composite membranes parallel to the preparation process it was possible to examine the development of the selectivities. A permselectivity P_{i-j} was defined as:

$$P_{i-j} = \left.\frac{\dot{n}_i}{\dot{n}_j}\right|_{\Delta p, \bar{p}, T} \tag{10}$$

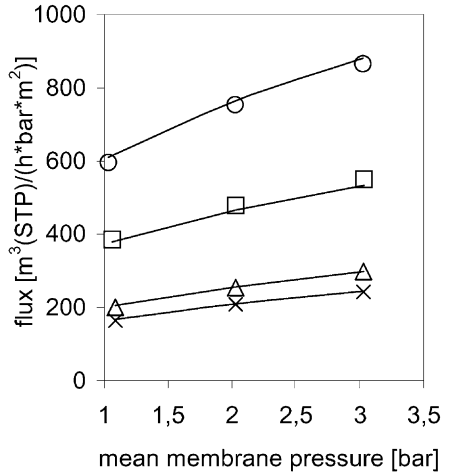

Fig. 10. Flux vs. pressure for the membrane consisting of the support and three layers at 25°C for hydrogen (○), helium (□), nitrogen (△), argon (×) (lines denote simulation with the determined parameters and symbols denote experimental data).

Table 4
Permselectivity of different gases for membranes with different layers

Membrane	P_{H_2-Ar}	$P_{H_2-N_2}$	P_{H_2-He}
Support	2.58	2.20	1.77
Support + 1st layer	2.81	2.33	1.76
Support + 1st + 2nd layer	3.14	2.62	1.58
Support + 1st + 2nd + 3rd layer	3.61	2.97	1.54
Support + 1st + 2nd + 3rd + 4th layer	3.79	3.16	1.43
Knudsen-selectivity ($\sqrt{M_j}/\sqrt{M_i}$)	4.47	3.74	1.41

Table 4 shows permselectivities P_{i-j} from the single component fluxes for different gas pairs and increasing numbers of layers. Due to the reduction of the mean pore diameter with each additional layer, the values of the permselectivities tend to reach the Knudsen-selectivities. The permselectivities for H_2–Ar and H_2–N_2 improve with each additional layer whereas P_{H_2-He} decreases. This behaviour can be understood analysing the effect of the pore diameter in the DGM. The following holds if d_P decreases (or the number of layers increases).

P_{i-j} increases if

$$\frac{\sqrt{M_j}}{\eta_j} > \frac{\sqrt{M_i}}{\eta_i}$$

P_{i-j} decreases if

$$\frac{\sqrt{M_j}}{\eta_j} < \frac{\sqrt{M_i}}{\eta_i} \tag{11}$$

The relevant ratios of the root of the molecular weights to the viscosities at ambient temperature and pressure are summarised in Table 5. The data are in complete agreement with the above discussion and the observations.

After determining and validating the DGM parameters of all alumina layers a theoretical study was

Table 5
Ratio of roots of molecular weights and viscosities (Eq. (11))

Gas	$\sqrt{M}/\eta$ ($\sqrt{\text{kg/mol}}$/Pa s)
Hydrogen	5034
Argon	8844
Nitrogen	9403
Helium	3228

Table 6
Simulated flow direction influence on flux for the examined alumina membrane (support and 4 layers)

Gas	Argon	Argon	Hydrogen	Hydrogen
Temperature (°C)	25	400	25	400
Flux (m^3/h bar m^2) (direction 1[a])	45.6	26.4	186.6	110.5
Flux (m^3/h bar m^2) (direction 2[b])	42.9	24.8	175.6	104.6
Ratio of fluxes	1.06	1.06	1.06	1.06

[a] Gas enters first the support.
[b] Gas enters first the last layer.

performed in order to quantify the effect of the direction of flow on the size of the overall fluxes. With the determined dusty gas model parameters of the support and the deposited layers, simulations were performed for the permeation of different single gases in both directions with the same overall pressure difference across the alumina membrane. In agreement with [14] for the asymmetric membranes considerable differences were obtained. In Table 6 typical results are depicted. Due to the local distribution of resistances in all cases the fluxes were found to be larger when the gas entered first the support. The differences of fluxes were about 6% which might be of practical significance.

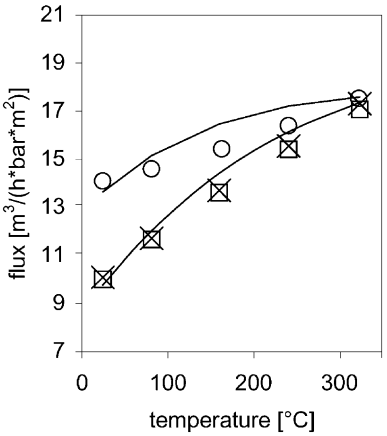

Fig. 11. Helium and hydrogen fluxes depending on temperature for a silica coated membrane for helium at 1.28 bar (□) and 2.26 bar (×) as well as for hydrogen (○) at 1 bar; lines-simulations with $E^{C}_{H_2} = 2968$ J/mol, $E^{C}_{He} = 4547$ J/mol, $\varepsilon/\tau\rho_g d_P(H_2) = 1.09 \times 10^{-8}$ m, $\varepsilon/\tau\rho_g d_P(He) = 2.08 \times 10^{-8}$ m (symbols denote experimental data).

Finally, permeation experiments with a silica coated alumina membrane were performed and analysed. The behaviour of the membrane completely changed after SiO_2-coating. In Fig. 11 the temperature dependence of the fluxes of helium and hydrogen is shown. In

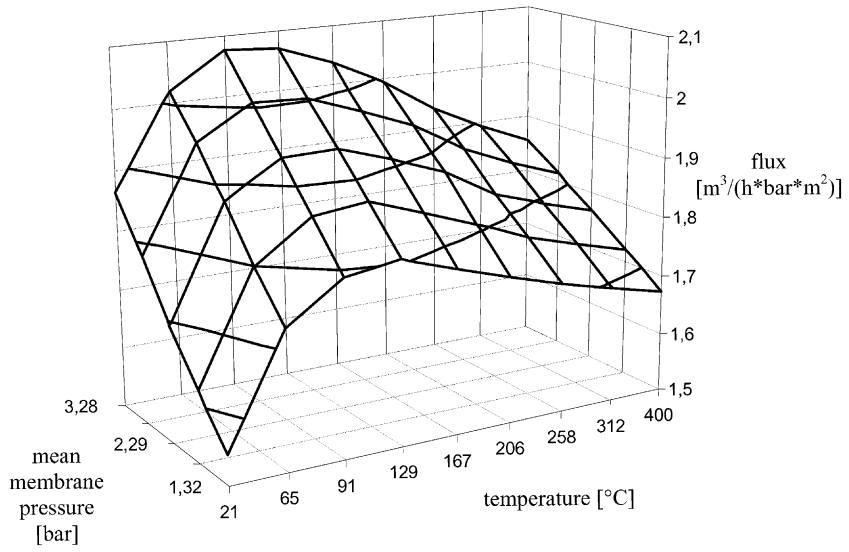

Fig. 12. Argon flux depending on temperature and pressure for a silica coated membrane.

contrast to the alumina membranes there is an increase of fluxes with increasing temperature and almost no effect of pressure. This could not be described by the DGM. A rough attempt to describe the mass transfer through all layers in an integral manner with Eq. (6) based on the concept of configurational diffusion allows to estimate corresponding activation energies, E^{C}. A linearisation ($\sqrt{T}\dot{n}/\Delta p$ versus $1/T$) was applied. The following values were determined: $E^{C}_{H_2} = 2968$ J/mol, $E^{C}_{He} = 4547$ J/mol. Eq. (6) describes the observed effects satisfactorily as can be seen in Fig. 11.

Fig. 12 illustrates the more complex behaviour of the fluxes of argon through the silica coated membrane as a function of temperature and mean membrane pressure. The experimental data are in the intersection points of the lines which are just guides to the eye. Due to the contribution of different mass transfer mechanisms it appears to be difficult to explore this behaviour completely. Obviously, also surface diffusion [22,23] plays an important role. Up to about 100°C the fluxes increase because of the mobility of adsorbed argon. At higher temperatures due to the reduced adsorption the fluxes decrease. The obvious influence of pressure might be partly attributed to the gas phase transfer through possible defects.

5. Conclusions

The mass transfer characteristics in asymmetric composite membranes were studied parallel to the preparation process. The results revealed that is was possible to analyse the essential transport mechanisms for the investigated multi-layer alumina membranes possessing relative large pores. The dusty gas model was capable to describe the overall transport in a wide parameter range for both flow directions. For the membranes studied and with the parameters obtained flux differences for the same total pressure of about 6% were calculated. The mass transfer through the finally deposited silica sol–gel layer was found to be much more complex. The observed temperature dependence of helium and hydrogen permeation gave evidence to an activated diffusion process.

The results obtained indicate that it appears to be on one side dangerous to use integral parameters to characterise composite membranes possessing several significant resistances. In particular, the aspect of flow direction dependencies of fluxes appears to be of importance in separation processes and for membrane reactor concepts. In the latter case also such questions whether a catalyst should be favourably placed inside or outside a tube are touched. On the other side it is obviously a formidable task to investigate such structures adequately and to explore the relevant transport mechanisms properly.

Acknowledgements

The authors thank P. Kölsch and M. Noack (ACA, Berlin) for stimulating discussions and experimental help. M. Stöhr (ACA, Berlin) is thanked for technical assistance. The authors thank Dr. Voigt and his co-workers (Hermsdorfer Institut für Technische Keramik) for the starting ceramic membranes, Dr. Weidner (BAM, Berlin) for gel-chromatography, Dr. Müller (ACA, Berlin) for ^{29}Si-NMR, Mrs. Sieber (HMI, Berlin) for FE-SEM and EDX. The BMBF is thanked for financing the project (Grants 03C0286 A6 and 03C0286 B9).

References

[1] H.P. Hsieh, Inorganic Membrane Separation Technology, Blackie, London, 1996.
[2] H. Weyten, J. Luyten, K. Keizer, L. Willems, R. Leysen, Catal. Today 56 (2000) 3–11.
[3] J.P. Collins, R.W. Schwartz, R. Sehgal, T.L. Ward, C.J. Brinker, G.P. Hagen, C.A. Udovich, Ind. Eng. Chem. Res. 35 (1996) 4398–4405.
[4] P. Quicker, V. Höllein, R. Dittmeyer, Catal. Today 56 (2000) 21–34.
[5] H. Weyten, K. Keizer, A. Kinoo, J. Luyten, R. Leysen, AIChE J. 43 (1997) 1819.
[6] J.E. ten Elshof, H.J.M. Bouwmeester, H. Verweij, Appl. Catal. A: General 130 (1995) 195.
[7] Y. Zeng, Y.S. Lin, S.L. Swartz, J. Membr. Sci. 150 (1998) 87.
[8] Y. Lu, A.G. Dixon, W.R. Moser, Y.H. Ma, U. Balachandran, Catal. Today 56 (2000) 297–305.
[9] J. Coronas, J. Santamaria, Catal. Today 51 (1999) 377–389.
[10] G. Saracco, H.W.J.P. Neomagus, G.F. Versteeg, W.P.M. van Swaaij, Chem. Eng. Sci. 54 (1999) 1997–2017.
[11] V. Gryaznov, Catal. Today 51 (1999) 391–395.
[12] Catalysis in Membrane Reactors, Catal. Today 56 (2000), special issue.
[13] P. Uchytil, J. Mater. Sci. 31 (1996) 6293–6298.

[14] P. Uchytil, O. Schramm, A. Seidel-Morgenstern, J. Membr. Sci. 170 (2000) 215–224.
[15] E.A. Mason, A.P. Malinauskas, Gas Transport in Porous Media: The Dusty-gas Model, Elsevier, Amsterdam, 1983.
[16] J. Kärger, D.M. Ruthven, Diffusion in Zeolites and other Microporous Solids, Wiley, New York, 1992.
[17] R. Krishna, J.A. Wesselingh, Chem. Eng. Sci. 52 (1997) 861.
[18] M.P. Hollowand, L.F. Gladden, Chem. Eng. Sci. 47 (1992) 1761–1770.
[19] J. Xiao, J. Wei, Chem. Eng. Sci. 47 (1992) 1123–1141.
[20] A.B. Shelekin, A.G. Dixon, Y.H. Ma, AIChE J. 41 (1995) 58–67.
[21] R.C. Reid, J.M. Prausnitz, B.E. Poling, The Properties of Gases and Liquids, McGraw Hill, New York, 1987.
[22] A. Tuchlenski, P. Uchytil, A. Seidel-Morgenstern, J. Membr. Sci. 140 (1998) 165–184.
[23] W.J.W. Bakker, L.J.P. van den Broeke, F. Kapteijn, J.A. Malign, AIChE J. 43 (1997) 2203–2214.
[24] C.J. Brinker G.W. Schemer, Sol–Gel Science, Academic Press, San Diego, 1990.
[25] R. de Vso, H. Verweij, Science 279 (1998) S1710.
[26] K. Croak, Z. Shogun, K. Obit, T. Kakitani, T. Yazawa, J. Membr. Sci. 160 (1999) 31–39.
[27] A. Tavolaro, E. Drioli, Adv. Mater. 11 (1999) 975–996.
[28] J. Caro, M. Noack, P. Kölsch, R. Schäfer, Micropor. Mesopor. Mater. 38 (2000) 3–24.
[29] P. Kölsch, M. Noack, P. Druska, D. Müller, P. Toussaint, J. Caro, Chem. Ing. Technol. 70 (1998) 850–866.
[30] M. Noack, P. Kölsch, P. Toussaint, P. Druska, J. Caro, Chem. Ing. Technol. 70 (1998) 992–998.
[31] M. Noack, P. Kölsch, U. Bentrup, P. Druska, P. Toussaint, J. Caro, Chem. Ing. Technol. 70 (1998) 1331–1336.
[32] J. Caro, M. Noack, P. Kölsch, Micropor. Mesopor. Mater. 22 (1998) 321.
[33] C.G. Guizard, A.C. Julbe, A. Ayral, J. Mater. Chem. 9 (1999) 55–65.